A model to simulate the moment-rotation and crack width of FRC members reinforced with longitudinal bars

Joaquim A. O. Barros
Full Professor, ISISE, Dept. of Civil Engineering, Univ. of Minho, Campus de Azurém, 4810-058 Guimarães, Portugal. E-mail: barros@civil.uminho.pt;

Mahsa Taheri
PhD Candidate, ISISE, Dept. of Civil Engineering, Univ. of Minho, Campus de Azurém, 4810-058 Guimarães, Portugal.E-mail: taheri.mahsa09@gmail.com

Hamidreza Salehian
PhD Candidate, ISISE, Dept. of Civil Engineering, Univ. of Minho, Campus de Azurém, 4810-058 Guimarães, Portugal. E-mail: h.r.salehian@gmail.com

Abstract

The present work describes a model for the determination of the moment-rotation relationship of a cross section of fiber reinforced concrete (FRC) elements that also include longitudinal bars for the flexural reinforcement (R/FRC). Since a stress-crack width relationship ($\sigma - w$) is used to model the post-cracking behavior of a FRC, the σ-w directly obtained from tensile tests, or derived from inverse analysis with three-point notched beam bending tests, can be adopted in this approach. For a more realistic assessment of the crack opening, a bond stress *vs.* slip relationship is assumed for the simulation of the bond between longitudinal bars and surrounding FRC. To simulate the compression behavior of the FRC, a shear friction model is adopted based on the physical interpretation of the post-peak compression softening behavior registered in experimental tests. By allowing the formation of a compressive FRC wedge delimited by shear band zones, the ambiguous concept of concrete crushing failure mode in beams failing in bending is reinterpreted. By using the moment-rotation relationship, an algorithm was developed to determine the force-deflection response of statically determinate R/FRC elements. The model is described in detail and its good predictive performance is demonstrated by using available experimental data. Parametric studies were executed to evidence the influence of relevant parameters of the model on the serviceability and ultimate design conditions of R/FRC elements failing in bending.

Keywords: Fiber reinforced concrete; Longitudinal steel bars; Moment-rotation response; Force-deflection response; Crack width.

1. Introduction

Recently a closed form analytical model was developed for the prediction of the moment-curvature relationship of fiber reinforced concrete (FRC) cross section of elements that can be also flexurally reinforced with longitudinal steel and fiber reinforced polymer (FRP) bars [1]. In the present work this type of elements will be designated as R/FRC. In that model, strain softening and strain hardening FRC composites [2] can be simulated by using a tensile stress-strain diagram, but its applicability, mainly in case of strain softening FRCs, can be arguable, since the formation of a predominant tensile failure crack just after crack initiation recommends the use of a stress-crack width relationship ($\sigma - w$) for modeling the post-cracking behavior of this type of materials. The use of tensile strain concept, instead of crack width, on the simulation of the post-cracking behavior of tensile strain softening FRCs requires the adoption of a characteristic length parameter [3] whose evaluation is still a controversial process. Furthermore, in the model of Taheri et al. [1] perfect bond conditions were assumed between longitudinal tensile bars and surrounding concrete in order to get a closed form approach for the formulation. However, experimental and advanced numerical simulations evidence the effect on the crack patterns and on the flexural response of R/FRC elements failing in bending when considering more realistic approaches for modeling the bond behavior [4, 5].

Concrete in compression is normally simulated by a stress-strain relationship determined from uniaxial compression tests under axial displacement control, but the post-peak softening response is dependent of several factors, like the geometry and size of the specimen, boundary conditions of the specimen in the testing phase, stiffness of the testing rig, test control conditions, and monitoring arrangement for the evaluation of the axial strain [6, 7]. Therefore, the post-peak compression phase is not a material response, and can be regarded as a structural behavior where the softening is mainly caused by the coalescence of micro- and meso-cracks into a shear failure crack governed by a coupled phenomenon of shear friction and crack opening [8]. This physical interpretation of the concrete behavior in compression is implemented in the numerical approach developed in the present work.

To estimate the average final crack spacing $\left(L_{csm}\right)$ and the design value of the crack width $\left(w_d\right)$ for members of steel fiber reinforced concrete (SFRC), including

longitudinal steel bars (R/SFRC) and subjected principally to flexure or tension, the RILEM TC 162-TDF [9] proposed the following equations:

$$L_{csm} = \left(50 + 0.25 k_1 k_2 \frac{\phi}{\rho_{s,ef}}\right)\left(\frac{50}{l_f / d_f}\right) \text{ (in } mm\text{)} \tag{1}$$

$$w_d = k_3 L_{csm} \varepsilon_{sm} \tag{2}$$

where ϕ is the bar diameter, $\rho_{s,ef}$ is the effective reinforcement ratio:

$$\rho_{s,ef} = \frac{A_s}{2.5cb} \tag{3}$$

being A_s the cross sectional area of the longitudinal reinforcement contained within the effective SFRC area in tension $A_{c,ef}$ =2.5cb, where c is the concrete cover and b is the width of the cross section. In Eq. (1) l_f / d_f is the fiber aspect ratio, where l_f and d_f is the fiber length and diameter, respectively. In Eq. (2) ε_{sm} is the mean strain in the reinforcement between cracks:

$$\varepsilon_{sm} = \frac{\sigma_{st}}{E_s}\left[1 - k_4 k_5 \left(\frac{\sigma_{sr}}{\sigma_{st}}\right)^2\right] \tag{4}$$

where σ_{st} is the stress in the reinforcement, E_s is modulus of elasticity of steel bars, and σ_{sr} is the maximum steel stress at crack section of the crack formation stage [10]:

$$\sigma_{sr} = \frac{\left(f_{ctm} - f_{Ftsm}\right)}{\rho_{s,ef}} \cdot \left(1 + \gamma_s \rho\right) \tag{5}$$

where f_{ctm} and f_{Ftsm} is, respectively, the average value of the tensile strength and the average value of the residual flexural tensile strength of FRC (f_{Fts}):

$$f_{Fts} = 0.45 f_{R1} \tag{6}$$

being f_{R1} the residual flexural tensile strength at a crack mouth opening displacement (CMOD) of 0.5 mm, evaluated from the force-CMOD relationship determined from three point notched beam bending tests carried out according to the recommendations of RILEM TC 162-TDF [9].

In Eq. (5) $\gamma_s = E_s / E_c$, where E_c is the SFRC Young's modulus, and ρ is the longitudinal reinforcement ratio ($= A_s / b(h-c)$, being h the height of the cross section. In Eqs. (1), (2) and (4) k_1 to k_5 are non-dimensional coefficients, whose values can be found elsewhere [9].

More recently the CEB-FIP Model Code 2010 [10] has proposed the following equation to determine the w_d for R/FRC members:

$$w_d = 2\{k_6.c + \frac{1}{4}.\frac{\phi}{\rho_{s,ef}}.\frac{(f_{ctm} - f_{Ftsm})}{\tau_{bm}}\}.\frac{1}{E_s}.(\sigma_{st} - k_7\sigma_{sr} + k_8\varepsilon_s E_s) \quad (7)$$

where $\rho_{s,ef}$ is the effective reinforcement ratio:

$$\rho_{s,ef} = \frac{A_s}{2.5(c + \phi/2)b} \quad (8)$$

τ_{bm} is the average bond strength between reinforcing bars and surrounding concrete:

$$\tau_{bm} = 1.8 f_{ctm} \quad (9)$$

ε_s is the strain of rebar at the onset of cracking, and σ_{st} and σ_{sr} have the same meaning already proposed by RILEM TC 162 TDF [9]. In the evaluation of the σ_{st} the effect of the fiber reinforcement should be taken into account. To evaluate the maximum crack spacing in R/FRC elements, the CEB-FIP Model Code 2010 [10] proposes the following equation:

$$L_{cs,\max} = k_6 c.\frac{1}{4}\frac{(f_{ctm} - f_{Ftsm})}{\tau_{bm}}.\frac{\phi_s}{\rho_{s,ef}} \quad (10)$$

In Eqs. (7) and (10) k_6 to k_8 are non-dimensional coefficients, whose values can be found elsewhere [10].

Both the RILEM TC 162 TDF [9] and CEB-FIP Model Code 2010 [10] propose the concept of residual flexural tensile strength parameters (f_{Rj}) to characterize the post-cracking behavior of FRC. These parameters are determined from the force-CMOD curves obtained from three point beam bending tests, whose typical relationship is depicted in Fig. 1. Based on the force values, F_j, corresponding to the $CMOD_j$ (j= 1 to 4), the f_{Rj} are determined from the following equation:

$$f_{Rj} = \frac{3F_j L}{2b h_{sp}^2} \tag{11}$$

where b (=150 mm) and L (=500 mm) is the width and the span of the specimen, respectively, and h_{sp} (=125 mm) is the distance between the tip of the notch and the top of the cross section.

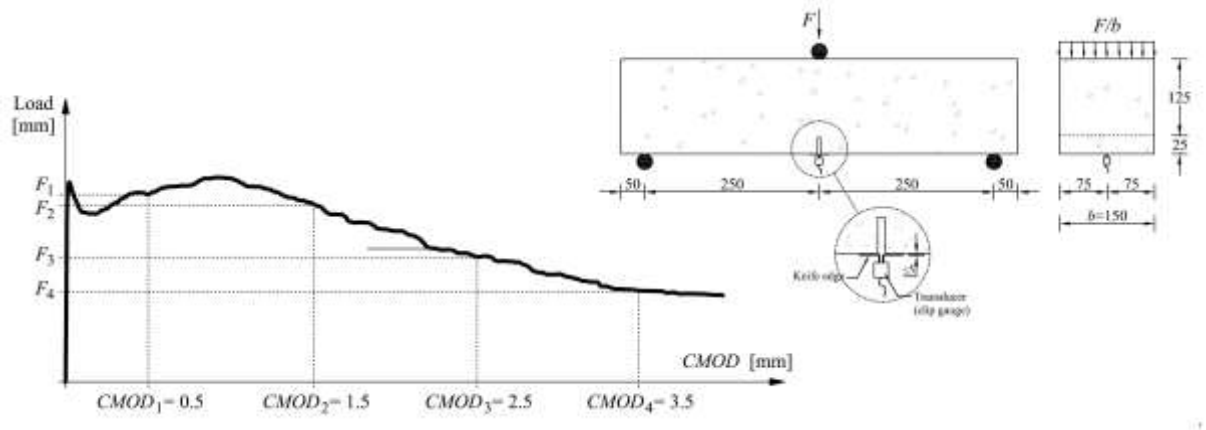

Fig. 1: Typical load versus– crack mouth opening displacement (CMOD) curve of FRC [10].

For structural applications with normal and high-strength concrete, the FRC classification proposed by CEB-FIP Model Code 2010 [10] is based on the post-cracking residual strength. For this purpose, the f_{R1k} (representing the strength interval) and a letter *a*, *b*, *c*, *d* or *e* (representing the f_{R3k} / f_{R1k} ratio) are considered. For instance (Fig. 2), a material denoted as "7b" has a strength f_{R1k} ranging between 7 and 8 MPa, and the f_{R3k} / f_{R1k} ratio ranging between 0.7 and 0.9.

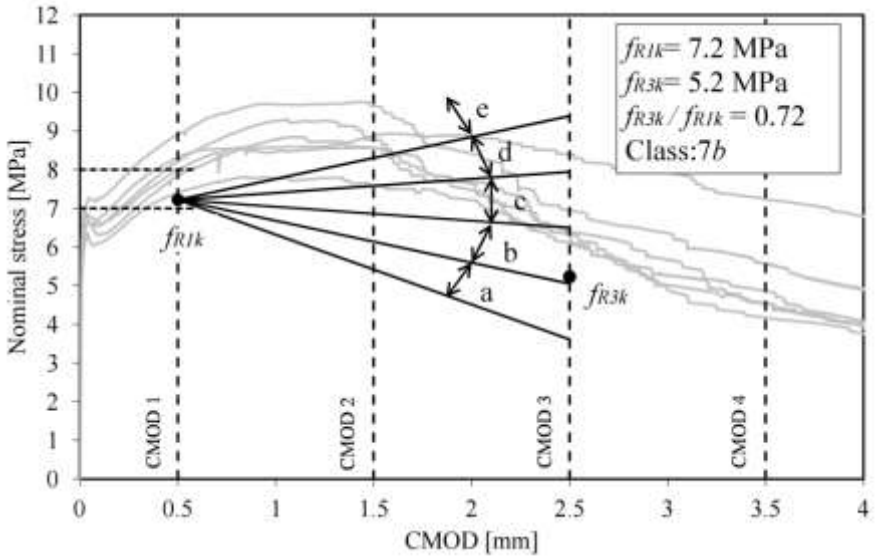

Fig. 2: The concept of toughness class for FRC based on the relationship between the flexural stress and CMOD [10].

In the present work a new approach is developed to determine the moment-rotation relationship of R/FRC elements failing in bending by considering the concepts proposed elsewhere [11-15] and adopting the following innovative aspects: 1) a $\sigma - w$ relationship to simulate the FRC post-cracking behavior; 2) a comprehensive interpretation of the behavior of the FRC in compression; 3) the bond between longitudinal bars and surrounding FRC. A simple approach is proposed to derive the force-deflection response of statically determinate R/FRC elements from the moment-rotation relationship of the sections of this type of elements. Using this model, a parametric study is carried out to assess the influence of the FRC toughness classes and bond stiffness on the behavior of R/FRC elements at serviceability and at ultimate limit states.

2. Numerical strategy for the evaluation of the moment-rotation and force-deflection of R/FRC beams failing in bending

2.1 Constitutive laws for the intervening materials

2.1.1 Tensile behavior of FRC

Fig. 3 represents the constitutive laws adopted to simulate the tensile behavior of FRC. Up to crack initiation the FRC is simulated by the following stress-strain equation:

$$\sigma_{ct}\left(\varepsilon_{ct}\right)=E_c\varepsilon_{ct} \quad \left(0\le\varepsilon_{ct}\le\varepsilon_{cr}\right) \tag{12}$$

where $\varepsilon_{cr}=f_{ct}/E_c$ is the strain at crack initiation, and f_{ct} and E_c are the tensile strength and Young's modulus of FRC that can be obtained from the recommendations of CEB-FIP Model Code 2010 [10]:

$$f_{ct}=\begin{cases}0.30\,f_{cc}^{2/3} & (for \le C50/60)\\ 2.12\ln\left(1+f_{cc}/10\right) & (for > C50/60)\end{cases} \tag{13}$$

$$E_c = 21.5\left(\frac{f_{cc}}{10}\right)^{1/3} \ (GPa) \tag{14}$$

being f_{cc} the concrete compressive strength in MPa. After crack initiation the FRC is described by a stress-crack opening diagram that can be formed by multi-linear segments (Fig. 3b) in order to have the potential of capturing, with high accuracy, the behavior of strain softening and strain hardening FRCs [1]:

$$\sigma_{ct}\left(w\right)=\left[\alpha_i+\left(\alpha_{i+1}-\alpha_i\right)\frac{w-w_i}{w_{i+1}-w_i}\right]f_{ct} \quad \left(for\ w_i<w\le w_{i+1}\right)$$
$$\left(i=0 \ \ to \ \ 6,\ \alpha_0=1,\ w_0=0,\ \alpha_6=0, w_6=w_u\right) \tag{15}$$

where $\alpha_i=\sigma_i/f_{ct}$ is the normalized stress parameter corresponding to crack width w_i, and w_u is the ultimate crack width. The shape of the $\sigma-w$ diagram can be determined by performing uniaxial tensile tests with notched FRC specimens [16, 17], or by inverse analysis by fitting with a target accuracy the force-crack mouth opening displacement (CMOD) registered in notched FRC beam bending tests [18]. Available experimental and numerical research evidence that a $\sigma-w$ diagram formed by four branches is capable of simulating with enough accuracy the post cracking behavior of the types of FRC being used in structural applications [9] . The CEB-FIP model code 2010 [10] defines a strategy to determine the $\sigma-w$ constitutive law for FRC by using the flexural tensile strength parameters obtained in three point FRC notched beam bending tests. This strategy has provided good predictions [18].

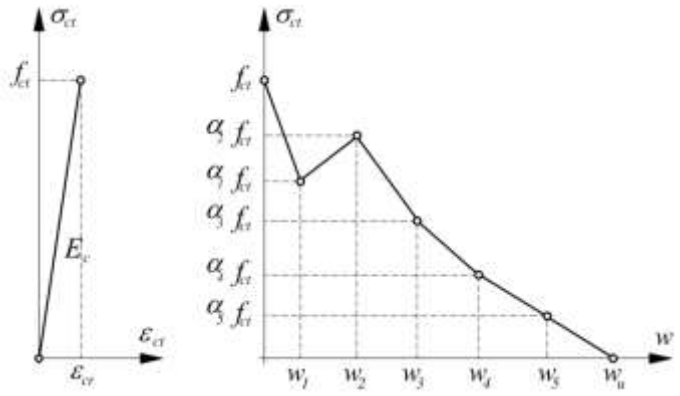

(a) (b)

Fig. 3: Tensile behavior of FRC: (a) linear stress-strain relationship before cracking, (b) Post-cracking stress-crack width response.

2.1.2 Compressive behavior of FRC

Fig. 4 identifies the four distinct consecutive stages of cracking that can be identified in concrete under uniaxial compressive load, based on initiation and propagation of cracks [19]:

- Stage I - below ≈30% of the peak stress. The initiation of internal cracks is insignificant, and the stress-strain relationship may be considered as linear;
- Stage II - between ≈30% and ≈80% of the peak stress. Firstly, the initial cracking at the interface zone (ITZ) starts to propagate and new micro-cracks develop. At approximately 60% of the peak stress, cracks at the cementitious matrix start to develop too. However, all these cracks are isolated and randomly distributed over the material volume;
- Stage III - between ≈80% and 100% of the peak stress. At this stage, all the small internal cracks become unstable and start to localize into major cracks. The crack growth is stable until peak is reached, what means that cracks only propagate if the load is increased. This phenomenon is referred as damage localization or strain localization;
- Stage IV - after the peak load. The major cracks continuously propagate, even though the load is decreasing. Unloading (snap-back) may occur at the material outside the damage zone, while the deformation at the localized damage band keeps increasing.

In fibrous concrete, the amplitude of the stages II and III is larger than the corresponding ones in plain concrete. This amplitude depends, mainly, on the fiber type and content. However, the main influence of the fiber reinforcement mechanisms is especially visible in the stage IV, where, depending on the fiber characteristics and concrete properties, a significant increase on the material energy absorption capacity can be obtained [20].

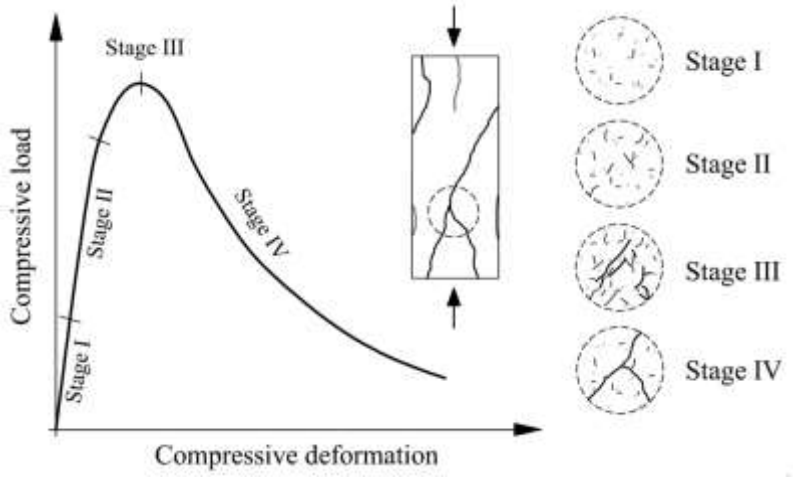

Fig. 4: Progress of damage in concrete under direct compression.

The most important idea to retain of the aforementioned mechanisms is the effect of the phenomenon of strain localization in concrete fracture behavior. Until load reaches ≈80% of peak load, only small isolated and randomly distributed cracks exist, and the distribution of stresses and strains can be reasonability predicted by continuous mechanics. With the increase of load, the subsequent coalescence of internal cracks into major cracks determines the damage and strain localization, converting fracture of concrete into a localized phenomenon. This invalidates the use of strain as state variable in constitutive laws for concrete [6]. Fracture mechanics should be used to describe the failure of concrete, since the localized damage band can be physically simulated by a crack. Stress and strain variables used to define the constitutive laws are, per definition, only valid at a macro-level of analysis and, consequently, unsuitable to describe localized phenomena, like the localization of cracking and shear-sliding in the post-peak regime. As soon as macro-cracks start to grow in the specimen, structural changes at a

scale of the order of the specimen size occur, and structural response is measured rather than pure material behavior in a representative volume.

Moreover, available experimental research on the characterization of the uniaxial concrete compressive behavior indicates that the response of the specimen in the stage IV depends of several factors, namely: boundary conditions of the specimen; size and shape of the specimen; monitoring system adopted to evaluate the strain; loading rate; test controlling conditions; stiffness of the testing rig. Therefore, the response determined in the post-peak phase should not be regarded as a material property, being eminently a structural response. To take this experimental evidence into account, in the present approach the compressive response is decomposed in two phases (Fig. 5): a pre-peak phase (including by simplification the stages I, II and III) characterized by a stress-strain law ($\sigma_{cc} - \varepsilon_{cc}$); a post peak phase (corresponding to the stage IV) simulated by a stress-deformation relationship ($\sigma_{cc} - u$), where the displacement, u, is the axial component of the sliding, S, in the shear band, as represented in Fig. 6.

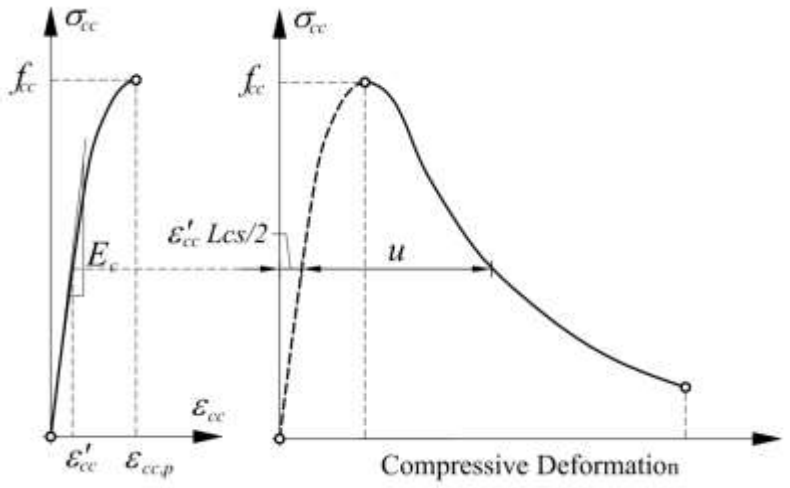

(a) (b)

Fig. 5: Compressive behavior of a FRC: (a) pre-peak stress-strain response, (b) post-peak stress-deformation response.

To simulate the pre-peak stress-strain response the equation proposed by Vipulanandan and Paul [21] was adopted:

$$\sigma_{cc}(\varepsilon_{cc}) = f_{cc}\frac{\varepsilon_{cc}/\varepsilon_{cc,p}}{(1-p-q)+q\left(\varepsilon_{cc}/\varepsilon_{cc,p}\right)+p\left(\varepsilon_{cc}/\varepsilon_{cc,p}\right)^{\frac{1-q}{p}}} \tag{16}$$

$$q = 1-p-\frac{E_{c,\sec}}{E_c},\ p+q\in]0,1[,\ \frac{1-q}{p}>0 \tag{17}$$

where $\varepsilon_{cc,p}$ is the strain corresponding to the concrete compressive strength $\left(f_{cc}\right)$, $E_{c,\sec}$ is the secant modulus of elasticity of concrete $\left(=f_{cc}/\varepsilon_{cc,p}\right)$, and p is a parameter ranging between 0 to 1. For hooked ends steel fibers similar to the ones used in the experimental programs considered in the present work for the assessment of the predictive performance of the proposed model, Barros and Figueiras [22], based on experimental research and inverse analysis procedure, proposed the following equations for the evaluation of $\varepsilon_{cc,p}$ and *p* parameters:

$$\varepsilon_{cc,p}^{SFRC} = \varepsilon_{cc,p}^{PC} + 0.0002W_f \tag{18}$$

$$p = 1.0 - 0.919\exp\left(-0.394W_f\right) \tag{19}$$

where W_f is the fiber weight percentage, and $\varepsilon_{cc,p}^{PC}$ is the strain at compressive strength of the plain concrete of the same strength class of the FRC [10]. The superscript *SFRC* and *PC* in Eq. (18) indicate that the entity is measured in specimens of steel fiber reinforced concrete and plain concrete of the same strength class, respectively.

The stage IV of the compressive behavior represented in Fig. 4 is simulated by the $\sigma_{cc}-u$ diagram schematically depicted in Fig. 5(b), where u is the axial displacement component of the shear sliding occurred in the contour of the wedge concrete submitted to compression (see Figs. 6). The formation of a concrete wedge in compression, delimited by shear band zones where the stress relieve in the concrete interior to the wedge is caused by the shear sliding and crack opening in the shear bands, permits a non-superposition of the material usually assumed for the concrete in compression when a full stress-strain relationship is adopted for the concrete in compression [23]. The shear sliding is accompanied by a crack opening due to the aggregate interlock effect. Due to the softening nature of the shear stress, τ_1, and normal stress, σ_1, with the increase of shear sliding and crack opening developed in the shear bands [24], the

compressive stress in the concrete interior to the wedge also decreases with the increase of the u displacement component.

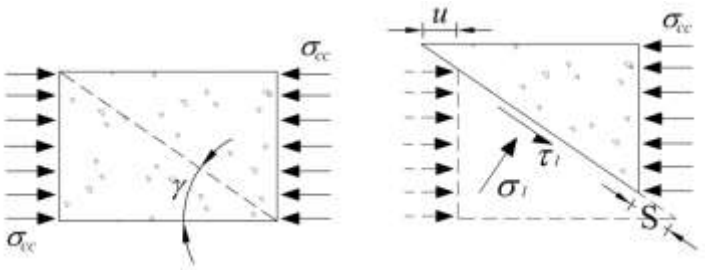

Fig. 6: Wedge sliding mechanism in compression.

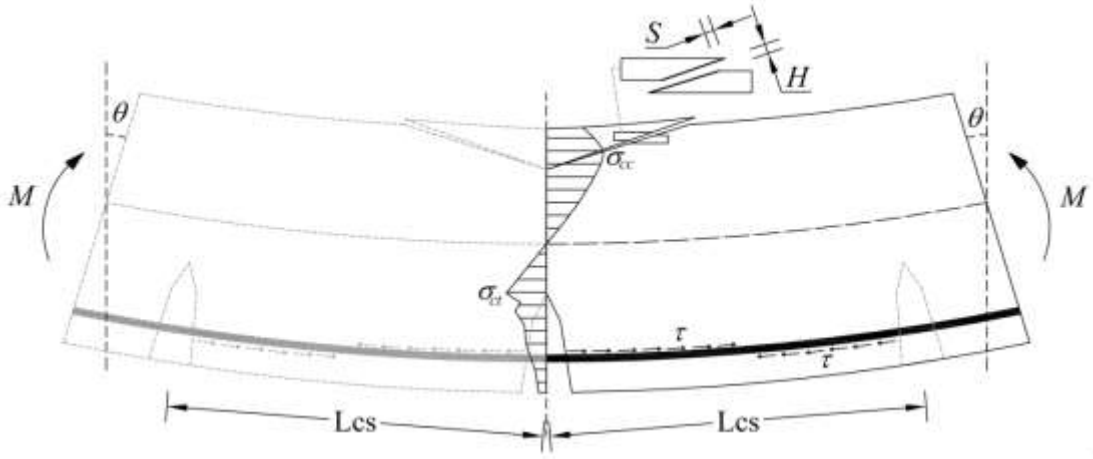

Fig. 7: Wedge sliding mechanism in a RC beam failing in bending.

The shear stress versus shear sliding, $\tau_1 - S$, depends on the normal stress σ_1 acting on the shear band, where for a certain $S = u/\cos\gamma$, the τ_1 increases with the normal stress component σ_1. The following equation can be used to simulate this type of behavior [23]:

$$\tau_1 = 0.497\, f_{cc} + \left(-30.142 + 51.623\frac{\sigma_1}{f_{cc}}\right)\left(\frac{u}{\cos\gamma}\right)\left(\frac{f_{cc}}{30}\right)^{0.91} \qquad (N \text{ and } mm) \qquad (20)$$

where γ is *the* concrete frictional angle, which is ranging between 37° and 57.5° for ordinary concrete depending on the concrete resistance [25]. Since no reliable

information is available on the effect of the fiber reinforcement on the γ value, the same interval is also assumed for FRC in the present work. Imposing equilibrium equations in both horizontal and vertical directions of the forces acting on the concrete wedge, the following equation is derived:

$$\sigma_{cc} = \left(\tan\gamma + \cot\gamma\right)\left(\frac{-30.142\left(\frac{u}{\cos\gamma}\right)\left(\frac{f_{cc}}{30}\right)^{0.91} + 0.497 f_{cc}}{\left(1-\left(51.623\frac{\tan\gamma}{f_{cc}}\right)\left(\frac{u}{\cos\gamma}\right)\left(\frac{f_{cc}}{30}\right)^{0.91}\right)}\right) \tag{21}$$

The influence of the concrete frictional angle (γ) on the compressive post-peak response of concrete is illustrated in Fig. 8a by considering two values for γ parameter, 37 and 47 degrees, and assuming a concrete of compressive strength of 60 MPa. It is verified that varying the γ parameter in an interval of values expected for concretes, the post-peak response of the concrete is not significantly affected. Furthermore, in Fig 8b are compared the post-peak responses of the concrete determined from the shear wedge sliding approach (Eq. 21) and from a conventional approach based on a stress-strain diagram (Eq. 16). According to Fig. 8b the shear wedge sliding approach leads a higher post-peak compressive resistance. For the concrete strength class considered and for the values adopted in this example, the maximum difference on the post-peak compressive resistance was limited to 14%.

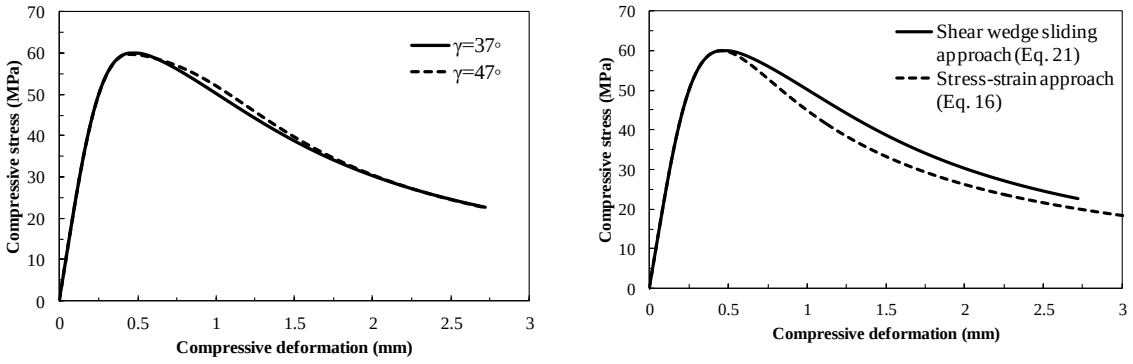

(a) (b)

Fig. 8: (a) Influence of the γ parameter on the concrete compressive post-peak response; (b) Comparison between compressive behaviour of concrete determined from shear wedge sliding and conventional stress-strain approach.

2.1.3 Tensile behavior of steel reinforcement

The elastic-perfectly plastic stress-strain response represented in Fig. 9 was considered to simulate the tensile behavior of the steel bars in tension:

$$\sigma_{st}\left(\varepsilon_{st}\right)=\begin{cases}E_s\varepsilon_{st} & \varepsilon_{st}\le\varepsilon_{sy}\\ f_{sy} & \varepsilon_{st}>\varepsilon_{sy}\end{cases} \tag{22}$$

where E_s is the modulus of elasticity, f_{sy} and ε_{sy} is the yielding stress and the corresponding strain, respectively, and ε_{su} is the ultimate tensile strain.

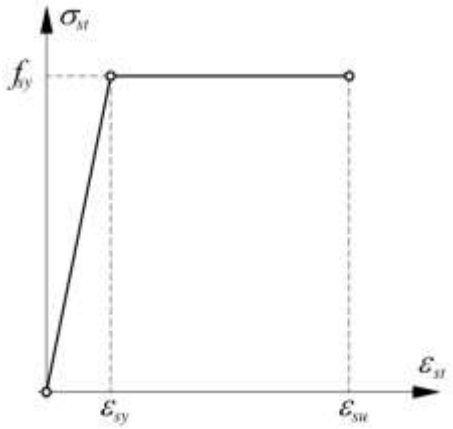

Fig. 9: Elastic-perfectly plastic response to simulate the tensile behavior of steel bars.

2.1.4 Bond stress-slip relationship to simulate the bond behavior between FRC and reinforcement

Based on equilibrium considerations, the following fundamental equation governing the bond between a steel bar and the surrounding concrete is determined [26]:

$$\frac{d^2s(x)}{dx^2}-\left(\frac{L_{ps}}{A_sE_s}+\frac{L_{ps}}{E_cA_{c,ef}}\right)\tau\left[s(x)\right]=0 \tag{23}$$

where A_s and L_{ps} is the cross section area and the perimeter of the reinforcement, respectively, $A_{c,ef}$ is the effective area of concrete in tension that can be defined according to the recommendations of CEB-FIP Model Code 2010 [10]. In the present

work $A_{c,ef}$ was assumed as the cross section area in tension, therefore its value is updated during the loading process in consequence of the variation of the neutral axis.

In the present version of the model, a simplified linear bond stress-slip relationship is assumed, but other more sophisticated laws can be adopted, only requiring more steps in the algorithm and more iterations for the convergence. Therefore, assuming a linear bond stress-slip relationship, $\tau = k_{bs}\, s$, the solution of Eq. (23) can be obtained from:

$$s(x) = A\cosh(\beta_s x) + B\sinh(\beta_s x) \tag{24}$$

where

$$\beta_s = \sqrt{k_{bs}\left(\frac{L_{ps}}{A_s E_s} + \frac{L_{ps}}{E_c A_{c,ef}}\right)} \tag{25}$$

being k_{bs} the bond stress-slip stiffness. The A and B constants in Eq. (24) are obtained by satisfying the boundary conditions in accordance to the bar-concrete sliding conditions between consecutive cracks, as schematically represented in Fig. 10.

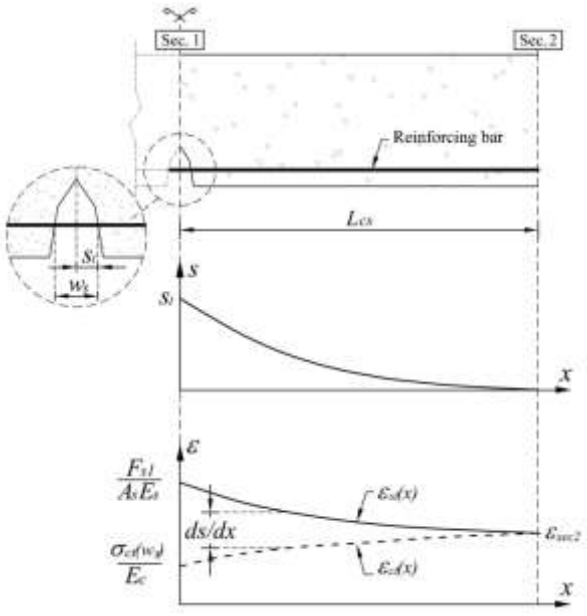

Fig. 10: Crack propagation and consequent sliding and strain distribution between cracks.

In the present approach it is assumed that the cracking formation process divides the beam in concrete prisms of a length L_{cs} that is the crack spacing.

In Fig. 10 is represented the variation along the bar-embedment length: the sliding, $s(x)$; concrete tensile strain, $\varepsilon_{ct}(x)=\sigma_{ct}\left[w_s\left(x\right)\right]/E_c$; and strain in the reinforcing bar, $\varepsilon_{st}(x)=F_s\left(x\right)/\left(A_sE_s\right)$, when the crack, of a crack width w_s, is formed in section 1 and just before the formation of the crack at section 2. For longitudinal bars crossed by flexural cracks the sliding of the bar at each face of the crack can be approximated as half of the crack width at the level of the reinforcement $\left(s(x=0)=s_1=w_s/2\right)$, as already considered by other researchers [23, 27]. In this approach the crack width is always assumed as being evaluated at the level of the tensile reinforcement. The sliding variation in section 1 is the difference between the strain in the reinforcement and in the surrounding concrete at this section:

$$\left.\frac{ds}{dx}\right|_{x=0}=\frac{F_{s1}}{A_sE_s}-\frac{\sigma_{ct}\left(w_s\right)}{E_c} \tag{26}$$

where F_{s1} is the force installed in the reinforcement at section 1, and $\sigma_{ct}\left(w_s\right)$ is the concrete tensile stress for a crack width w_s, evaluated from the stress-crack width diagram attributed to the FRC (Fig. 3b).

Sliding value and sliding variation tend to zero at section 2 $\left(s(x=L_{cs})=0\right.$; $\left.ds(x=L_{cs})/dx=0\right)$, where perfect bond conditions between reinforcement and surrounding concrete are assumed. Imposing these bond conditions to Eq. (24), the crack spacing of two adjacent cracks, which is the distance between sections 2 and 1, is obtained by assuming the following equation, whose deduction is detailed in [28]:

$$L_{cs}=\frac{2}{\beta_s} \tag{27}$$

2.2. Algorithm to predict the moment–rotation response of FRC hybrid reinforced cross section

A segment of a FRC beam flexurally reinforced with longitudinal bars, herein designated as R/FRC, with a length equal to the crack spacing, L_{cs}, is subjected to a pure bending moment M, as schematically represented in Fig. 11. When the most tensioned concrete surface (in Fig. 11 is the bottom surface) attains the concrete strain at crack initiation, $\varepsilon_{ct} = \varepsilon_{cr}$, i.e., when cracking bending moment is installed $\left(M = M_{cr}\right)$, a flexural crack is initiated, and due to symmetry only half part of the beam's segment is represented in Fig. 11. By increasing the rotation θ at the extremities of the beam's segment, the crack propagates towards the top surface of the beam. A symmetric cross section that can have a width varying along its depth (Fig. 11b), and a height *h*, is discretized in *n* layers in order to take into account the appropriate constitutive law for each concrete layer during the loading procedure. The width, the thickness and the depth of the i^{th} layer (with respect to the beam's top surface) is designated, respectively, by b_i, t_i, and d_i. For the concrete layer at the level of the reinforcement $\left(d_i = d_s\right)$ the total width of this layer $\left(b_i\right)$ is decomposed in the part corresponding to the reinforcement b_s $\left(b_s = A_s / t_i\right)$ and to the concrete b_c $\left(b_c = b_i - b_s\right)$.

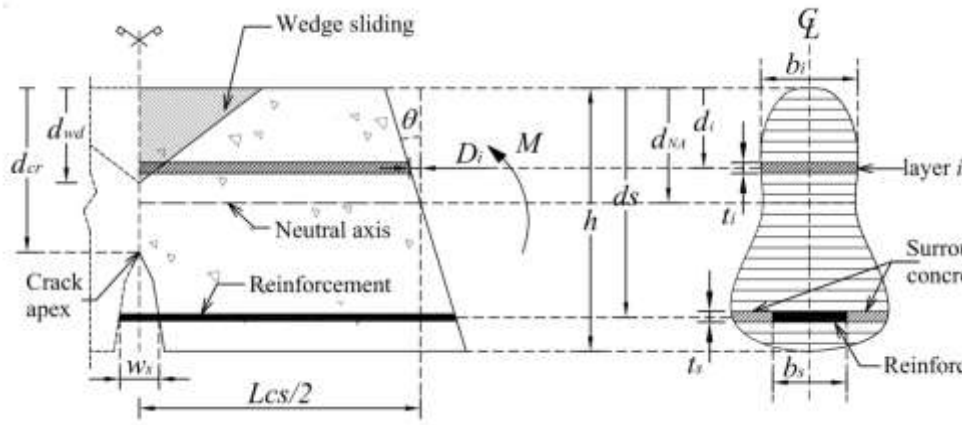

(a) (b)

Fig. 11: (a) Cracked R/FRC segment of length L_{cs} submitted to pure bending, (b) layer approach to discretize the cross section.

In the developed incremental-iterative algorithm (the increment is the rotation, while the iterative procedure is executed up to assure force equilibrium according to an adopted tolerance), the rotation of the beam in a k^{th} generic step of the computation is imposed by considering a constant increment of $\Delta\theta$:

$$\theta_k = k\Delta\theta \tag{28}$$

For this rotation, the axial displacement of the i^{th} layer, D_i^k, is determined by considering its position, d_i, and the distance of the neutral axis (d_{NA}):

$$D_i^k = \theta_k \left| d_i - d_{NA} \right| \tag{29}$$

while its corresponding effective strain is obtained from the following equation (the superscript *k* representing the loading step will be not indicated hereafter in order to simplify the notation):

$$\varepsilon_i^{ef} = \frac{2D_i}{L_{cs}} \tag{30}$$

where L_{cs} is the spacing between cracks obtained from Eq. (27). If $d_i < d_{NA}$ the compressive force in the i^{th} layer, F_i^c, can be obtained from the following equation:

$$F_i^c = \begin{cases} \sigma_{cc}\left(\varepsilon_i^{ef}\right) b_i t_i & if\ \varepsilon_i^{ef} \le \varepsilon_{cc,p} \\ \sigma_{cc}\left(u_i\right) b_i t_i & if\ \varepsilon_i^{ef} > \varepsilon_{cc,p} \end{cases} \tag{31}$$

where u_i is the horizontal component of i^{th} layer sliding, S_i, of the concrete wedge in compression softening, which is determined by solving the following system of equations:

$$\begin{cases} \varepsilon_i^{ef} - \varepsilon'_{cc,i} - \left(2u_i / L_{cs}\right) = 0 \\ \sigma_{cc}\left(u_i\right) - \sigma_{cc}\left(\varepsilon'_{cc,i}\right) = 0 \end{cases} \tag{32}$$

where $\varepsilon'_{cc,i}$ is the compressive strain of the layer when subjected to the axial displacement u_i (see Fig. 5b).

If $\left(d_i \ge d_{NA}\right)$ the tensile force in the i^{th} layer, F_i^c, can be obtained from the following equation:

$$F_i^c = \begin{cases} \sigma_{ct}\left(\varepsilon_i^{ef}\right) b_i t_i & if\ \varepsilon_i^{ef} \le \varepsilon_{cr} \\ \sigma_{ct}\left(w_i\right) b_i t_i & if\ \varepsilon_i^{ef} > \varepsilon_{cr} \end{cases} \tag{33}$$

where the tensile stress, $\sigma_{ct}\left(\varepsilon_i^{ef}\right)$, is obtained from the diagram represented in Fig. 3(a), while w_i is the crack width determined by solving iteratively the following equation:

$$w_i = \left[2D_i - \frac{\sigma_{ct}\left(w_i\right)}{E_c} L_{cs} \right] \tag{34}$$

The approach subjacent to Eq. (34) assumes that the crack width of the formed crack plus the deformation of the concrete along the prism ($\sigma_{ct}\left(w_i\right) L_{cs} / E_c$) is equal to total displacement of the cracked concrete at this level ($2D_i$).

To evaluate the force installed in the reinforcement $\left(F_i^s\right)$, two conditions should be considered:

i) when the reinforcement is not crossed by the crack ($d_s \le d_{cr}$, see Fig. 11a): in this case perfect bond conditions are assumed for the reinforcement, thereby the force is determined from the following equation:

$$F_i^s = b_s t_i \sigma_{st}\left(\varepsilon_i^{ef}\right) \tag{35}$$

ii) when the reinforcement is crossed by the crack ($d_s > d_{cr}$, see Fig. 11a): in this case the F_i^s is obtained by considering the bond stress-slip model described in Section 2.1.4, resulting the following equation [28]:

$$F_i^s = \frac{A_s E_s \left[s_1 \beta_s E_s + 0.76 \sigma_{ct}(w_s) \right]}{0.76 E_c} \tag{36}$$

By imposing the equilibrium of the axial forces in the cross section, the depth of the neutral axis, d_{NA}, is determined. For this equilibrium configuration corresponding to the k^{th} loading step, the bending moment is evaluated:

$$M_k = \sum_{i=1}^{n} F_i^c d_i + F_i^s d_s \tag{37}$$

where n is the number of layers of the cross section. Eqs. (28) and (37) define a point of the moment-rotation relationship, $M_k - \theta_k$. The moment-curvature response can also be obtained, $M_k - \chi_k$, where the curvature is determined from:

$$\chi_k = \frac{\varepsilon_{cc,1}}{d_{NA}} \tag{38}$$

being $\varepsilon_{cc,1}$ the concrete compressive strain at the top surface of the cross section. The flowchart of the algorithm is described in Fig. 12.

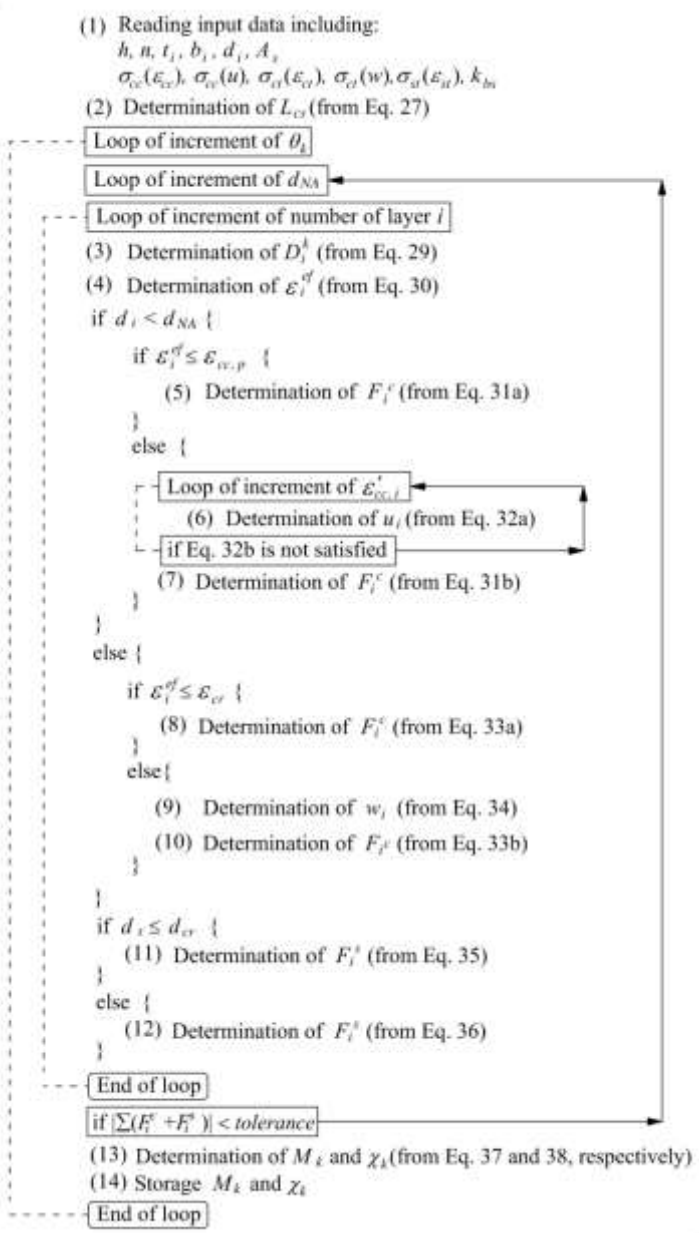

Fig. 12: Flow chart of the algorithm of the model.

2.3. Evaluation of force-deflection relationship

The force-deflection response of statically determinate beams failing in bending is determined by the algorithm schematically represented in Fig. 13. To evaluate the force-deflection response of a RC beam (or a slab's strip), the structural element is decomposed in m segments of length Δx. The moment-rotation relationship for each segment Δx representative of the beam (in terms of cross section geometry, materials and flexural reinforcement) is determined, and then converted in a moment-curvature relationship according to Eq. (38), since curvature is not dependent of the length of the adopted segments. The bending moment in the middle section of the i^{th} segment at a distance x_i from the left support $\left(M_k(x_i)\right)$ can be obtained for each increment of the imposed load configuration $\left(P_k\right)$.

By using the moment-curvature relationship for the cross section representative of each segment, obtained according to the model described in Section 3, the curvature $\left(\chi_k^i\right)$ and the corresponding flexural stiffness $\left(EI_k^i\right)$ for the $M_k(x_i)$ are determined. By applying the principle of virtual work, the mid-span deflection of the beam for the k^{th} loading step $\left(\delta_k\right)$ is obtained, resulting a P_k - δ_k point of the force-deflection response of the beam [29].

In [28] it is demonstrated that the length adopted for Δx in the algorithm of Fig. 13 has no effect on the force-deflection response, as long as it is adopted a number of segments capable of representing the types of sections of the structural element to simulate, as well as the variation of the bending moment.

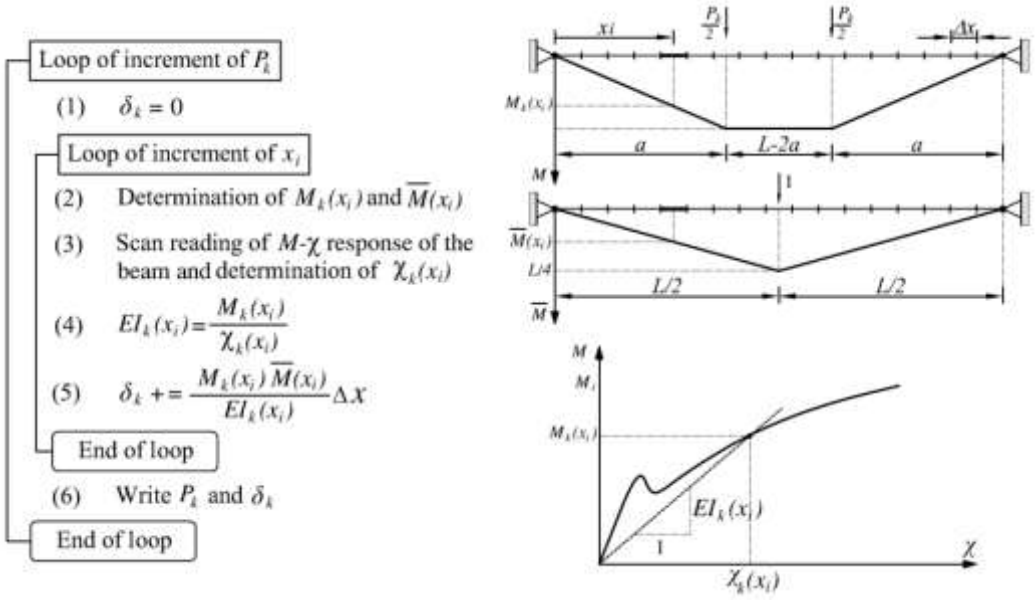

Fig. 13: Numerical approach to determine the force–deflection response of statically determinate beams failing in bending [29].

3. Model appraisal

The performance of the proposed model in terms of predicting the force-deflection response is evaluated by simulating the force-deflection relationship in R/FRC beams tested by Barros *et al.* [30].

The parameterized geometry and reinforcement arrangement of the beams of the three simulated experimental programs are represented in Fig. 14, and the corresponding data is indicated in Table 1. In these three experimental programs SFRC was used, and a four point loading configuration was adopted.

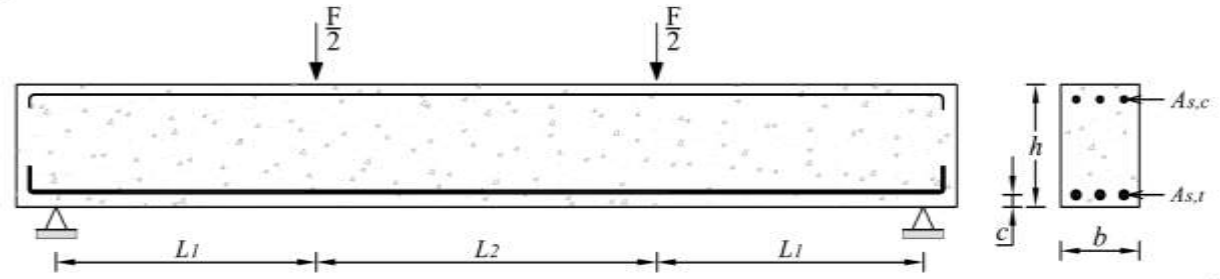

Fig. 14: Reinforced SFRC beam under four point loading configuration (data included in Table 1).

Table 1: Geometric properties of the beams (Fig. 14)

Beam series	Reference	b [mm]	h [mm]	c [mm]	L_1 [mm]	L_2 [mm]	$A_{s,t}$ [mm^2]	$A_{s,c}$ [mm^2]
B1							84.8	
B2	Barros *et al.* [30]	350	150	20	450	450	150.8	84.8
B3							235.6	
B4	Vandewalle [31]	200	350	35	750	1750	628.3	-
B5	Tan *et al.* [32]	100	125	25	665	665	157.1	-

The B1, B2, and B3 beams were made by a concrete reinforced with 45 kg/m^3 of hooked ends steel fibers of a length and diameter of 60 and 0.75 mm, respectively. The concrete compressive strength and the yield stress of the longitudinal steel bars are the relevant available information. To derive the constitutive law for defining the tensile behavior of SFRC, an inverse analysis procedure was executed by matching, as much as possible, the force-deflection response registered experimentally in the B1 beam. The obtained data is included in Table 2. The Young's modulus was determined from Eq. (14) for SFRC utilized in B1-B3 for both in tension and in compression. For the k_{bs} bond stiffness the value 70 MPa/mm was used.

In Fig. 15 the force-deflection response of B1, B2 and B3 beams, obtained by the developed numerical strategy, is compared to the corresponding one registered experimentally, being evident the good predictive performance of the model.

Table 2: Mechanical properties of intervening materials of the simulated beams

Beam series	f_{cc} [MPa]	f_{ct} [MPa]	α_1 -	α_2 -	α_3 -	α_4 -	α_5 -	w_1 [mm]	w_2 [mm]	w_3 [mm]	w_4 [mm]	w_5 [mm]	w_u [mm]	f_{sy} [MPa]	ε_{su} [‰]
B1														600	10
B2	99.2	2.53	0.86	0.83	0.64	0.36	0.27	0.01	0.1	0.3	0.6	1.8	3.0	670	15
B3														680	12
B4	37.5	2.49	1.11	0.57	0.49	0.40	0.31	0.016	0.40	1.10	1.80	2.49	2.55	500	15
B5	34.5	2.49	1.11	0.56	0.48	0.39	0.31	0.011	0.42	1.09	1.76	2.45	2.55	500	15

E_s = 200 GPa

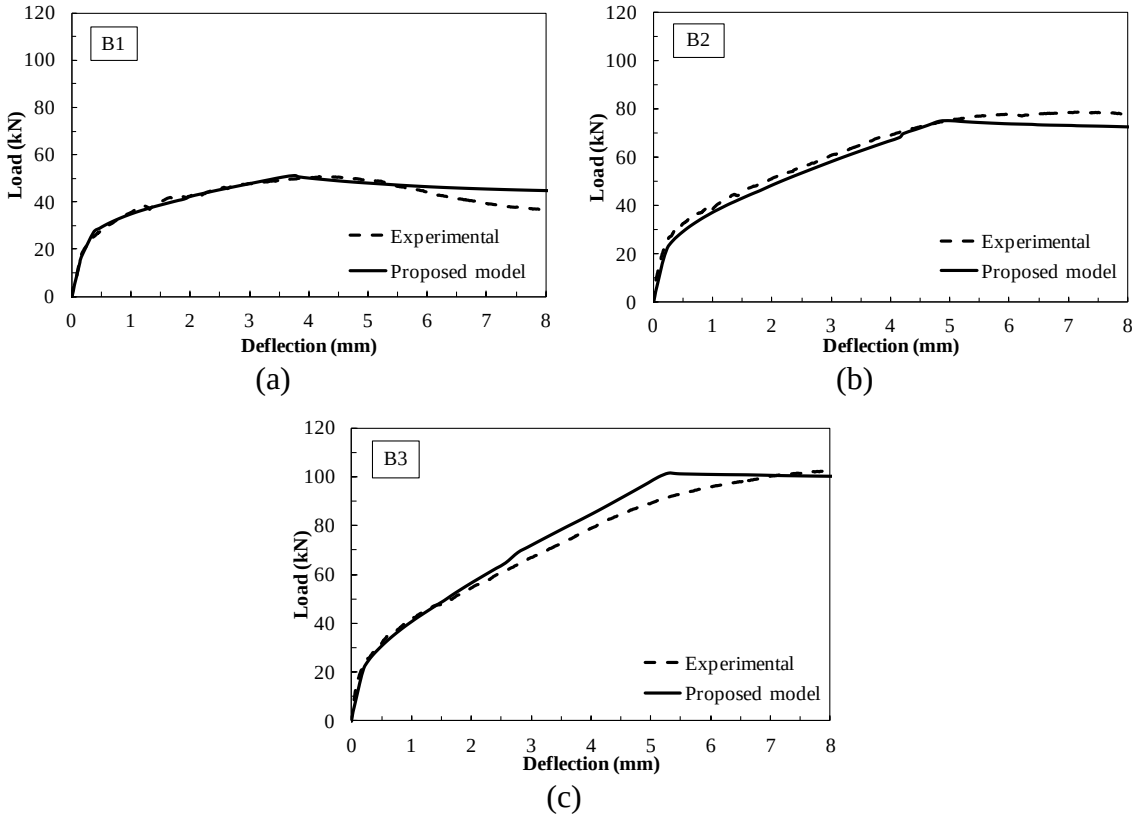

Fig. 15: Load-deflection response predicted by the proposed model and recorded in the experimental program.

The capability of the model to predict the crack width is also assessed by simulating the tests carried out by Vandewalle [31], and Tan *et al.* [32], whose test samples were made by SFRC with, respectively, 45 and 40 kg/m^3 hooked ends steel fibers of a length and diameter of 35 and 0.54 mm, designated in Table 1 by B4 and B5. Material properties of SFRC of beams B4 and B5 are indicated in Table 2, in which, due to lack of information about the post-cracking response of the utilized SFRC in these two experimental programs, CEB-FIP Model Code 2010 [10] recommendations were adopted to characterize the SFRC of these beams. For this purpose, the residual flexural strength parameters f_{R1} and f_{R3} were estimated according to the volume percentage (V_f) and geometry of the fibers (l_f = fiber length, d_f = fiber diameter) by using the following equations proposed by Moraes-Neto *et al.* [33]:

$$f_{R1} = 7.5\left(V_f \frac{l_f}{d_f}\right)^{0.8} \tag{39}$$

$$f_{R3} = 6.0\left(V_f \frac{l_f}{d_f}\right)^{0.7} \tag{40}$$

Table 2 includes the data derived according to this strategy to determine the tensile behavior of the SFRC of B4 and B5 beams. The value of 85 MPa/mm was considered for the bond stiffness parameter, k_{bs}. Fig. 16 shows that the model is capable of predicting with good accuracy the moment versus crack width response.

This figure also includes the moment-crack width relationship obtained by using the approaches proposed by RILEM TC 162-TDF [9] (Eqs. (1)-(6)) and Model Code 2010 [10] (Eqs. (7)-(9)). In the RILEM approach it was considered k_1=0.8, k_2=0.5, k_3=1.7, k_4=k_5=1.0. For the evaluation of ε_{sm} in Eq. (4) and the strain and stress values in the reinforcement by using Eq. (7) (σ_{st}, σ_{sr}, ε_s), the numerical approach proposed in the present work was also used. The average bond strength, τ_{bm}, was calculated using Eq. (9) and by adopting the average concrete tensile strength (f_{ctm}) indicated in Table 2. The f_{Fts} was obtained from Eq. (6) by considering the values for the f_{R1} calculated by Eq. (39). From the obtained results it is notable that the proposal of RILEM TC 162-TDF [9] predicts with high accuracy the crack width variation, as long as the average strain in the tensile reinforcement, which changes during the loading process, is determined by the numerical approach proposed in the present paper.

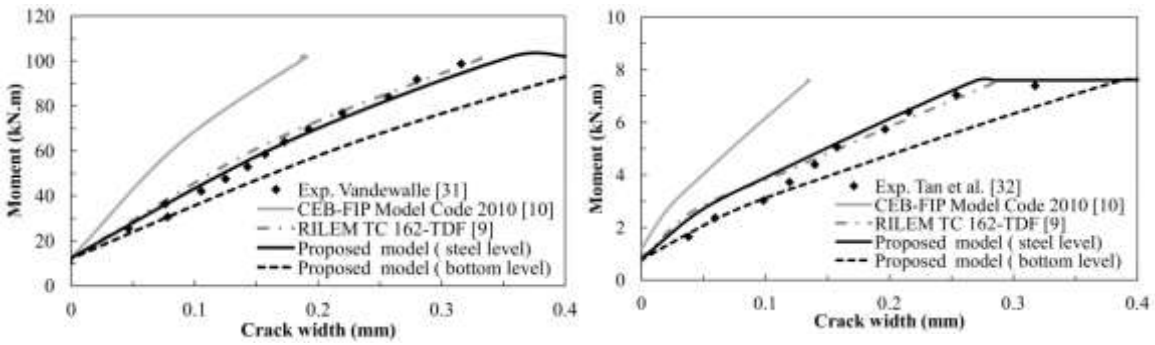

(a) (b)

Fig. 16: Predictive performance of the model in terms of moment-crack width response.

4. Parametric study

The numerical model is now used to assess the influence of the post-cracking performance of FRC on the load carrying capacity and cracking behavior of R/FRC beams. For this purpose, the post-cracking performance of FRC is classified according to the CEB-FIP Model Code 2010 [10] recommendations, a subject already introduced in "Introduction" section, and the four toughness classes of FRC indicated in Table 3 are adopted. This parametric study is applied to simply supported R/FRC beams of 2500 mm span length and rectangular cross section of 300 ×150 mm. A longitudinal reinforcement ratio of 0.5% was adopted by using steel bars of 16 mm diameter in the tension region, with a concrete cover of 50 mm. A FRC of compressive strength of 60 MPa was used, while for the longitudinal steel bars a yield stress $\left(f_{sy}\right)$ of 500 MPa, a modulus of elasticity $\left(E_s\right)$ of 200 GPa, and ultimate strain $\left(\varepsilon_{su}\right)$ of 11.5‰ were considered.

Table 3 – Toughness classes according to the CEB-FIP Model Code 2010 [10].

Case study	Toughness classification	Interval of f_{R1} [MPa]	Interval of f_{R3} / f_{R1}
FRC1	6a	[6,7]	[0.5-0.7]
FRC2	6d	[6,7]	[1.1-1.3]
FRC3	12a	[12,13]	[0.5-0.7]
FRC4	12d	[12,13]	[1.1-1.3]

By considering these values and adopting the methodology recommended by CEB-FIP Model Code 2010 [10] to define the post-cracking behavior of FRC (Fig.17), the influence of the toughness classes of FRC on the force-deflection and on the force-crack width response of the beams is represented in Fig. 18(a) and 18(b), respectively (two vertical dotted lines are represented in Fig. 18(b), corresponding to the maximum crack width limits imposed by CEB-FIP Model Code 2010[10],: 0.1 and 0.3 mm). The crack width was determined at the level of the longitudinal tensile reinforcement.

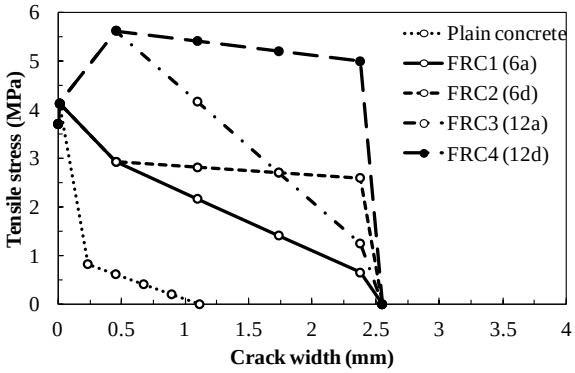

Fig. 17: Post-cracking diagrams of FRC of different toughness classes.

According to these figures, by varying the toughness class from 6a to 6d, and also from 12a to 12d has no effect on the service load (load level up to a crack width limit of 0.3mm, Fig. 18b). This means that the increase of the f_{R3}/f_{R1} ratio for a FRC of a certain f_{R1} has negligible effect in terms of load carrying capacity for service load conditions. However, for the present R/FRC beams an increase of 20.1% was obtained for the service load level corresponding to a crack width of 0.3mm when a FRC of f_{R1}=12MPa is used instead of a FRC of f_{R1}=6MPa. When compared to the adopted plain concrete of the same strength class, an increase of 42.8% and 71.5% was obtained in terms of load carrying capacity at serviceability limit conditions due to cracking when a FRC of f_{R1} equal to, respectively, 6 and 12 MPa is used.

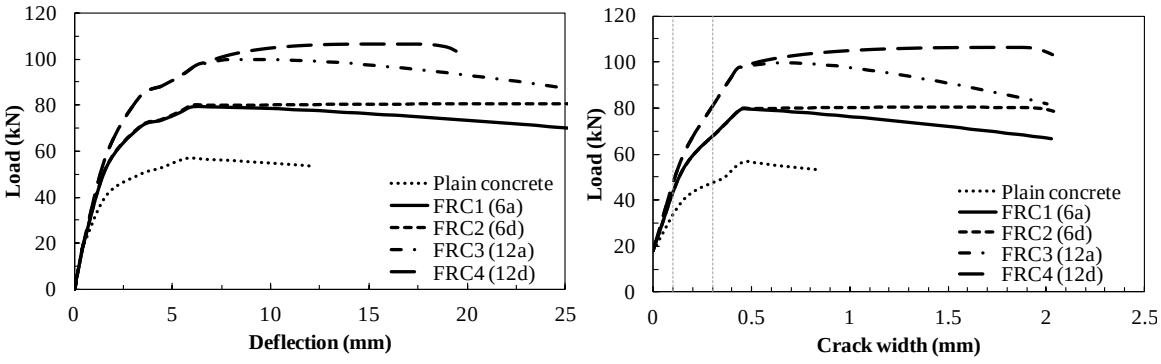

(a) (b)

Fig. 18: Influence of the FRC toughness class on the: (a) load-deflection, and (b) load-crack width responses of R/FRC beams.

Considering the material model properties of FRC3 (Table 3), the influence of the k_{bs} bond stiffness is evaluated in Fig. 19 by adopting a very stiff value (k_{bs} =80 MPa/mm), which simulates high bond conditions, and two other smaller values simulating higher sliding between reinforcement and surrounding concrete (k_{bs} = 15 and 7 MPa/mm). As Fig. 19(a) shows, for the interval of values considered for the k_{bs}, and assuming that a linear response for the bond stress versus slip is acceptable, which is the hypothesis considered in the present version of the model, the bond stiffness has no appreciable influence on the load-deflection response up to peak load, but for deflection levels higher than the one corresponding to the peak load, the load carrying capacity increases with k_{bs}. Both the peak load and its corresponding deflection increase with k_{bs}. The highest benefit of increasing k_{bs} is, however, on the load carrying capacity of the R/FRC for serviceability limit conditions due to maximum crack width restrictions (Fig. 19b). This figure clearly evidences that the load carrying capacity for this interval of crack width (0.1 to 0.3mm) increases with k_{bs}. The increase of the bond stiffness can be attained by including micro- and meso-fibers in the FRC composition, capable of minimizing the crack opening and propagation in the concrete surrounding the tensile steel bars [34]. In the present parametric studies it is verified that the increase of k_{bs} from 7 MPa/mm to 80 MPa/mm has provided an increase of 38.9% and 53.7% on the load carrying capacity for a crack width of, respectively, 0.1 and 0.3 mm.

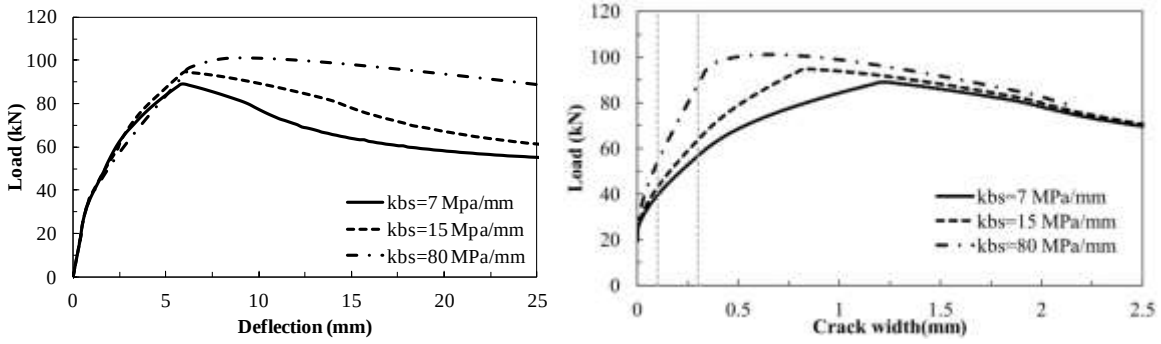

(a) (b)

Fig. 19: Effect of the k_{bs} bond stiffness on the: (a) load-deflection, and (b) load-crack width responses of R/FRC beams.

5. Conclusions

In the present paper an innovative numerical approach was developed to determine the moment vs. rotation relationship of cross section of fiber reinforced concrete (FRC) elements failing in bending. These elements can also include flexural tensile steel bars (R/FRC). The following novelties were implemented: a stress-crack width relationship for modeling the post-cracking behavior of R/FRC; a new approach to simulate the FRC in compression by using a stress-strain equation up to the strain corresponding to the compressive strength, and then a stress-deformation relationship based on the shear friction theory; a bond model to simulate the sliding between longitudinal tensile bars and surrounding FRC. By using the moment-rotation relation obtained from this approach, an algorithm was proposed to derive the force-deflection of statically determinate R/FRC elements. The good predictive performance was demonstrated by using available experimental data in terms of force-deflection and moment-crack width. By performing parametric studies with the developed numerical model, it was verified that in R/FRC elements of a longitudinal reinforcement ratio of 0.5% (a convenient ratio when fibers and longitudinal tensile bars are used) the flexural capacity for crack width limits imposed by actual design guidelines for the accomplishment of the serviceability limit states has increased significantly with the increase of the residual flexural tensile strength parameter for a CMOD=0.5 mm, f_{R1}. However, the other parameter that defines the toughness class of a FRC according to the CEB-FIP Model Code 2010[10], f_{R3}/f_{R1}, had only a beneficial effect on the flexural capacity for crack width values above the one corresponding to the yield initiation of the longitudinal reinforcement. Finally, it was observed that the bond stiffness has a quite favorable effect on the flexural capacity and on the arrestment of the crack opening up to the yield initiation of the longitudinal reinforcement.

Acknowledgements

This work is supported by FEDER funds through the Operational Programme for Competitiveness Factors – COMPETE and National Funds through FCT – Portuguese

Foundation for Science and Technology under the project PTDC/ECM/105700/2008 – "DURCOST - Innovation in reinforcing systems for sustainable pre-fabricated structures of higher durability and enhanced structural performance". The second and third author wish to acknowledge the grant provided by this project and FCT (SFRH/BD/71934/2010), respectively.

References

[1] Taheri M, Barros JAO, Salehian H. A design model for strain-softening and strain-hardening fiber reinforced elements reinforced longitudinally with steel and FRP bars. Composites Part B: Engineering. 2011;42:1630-40.

[2] Naaman AE, Reinhardt HW. Proposed classification of HPFRC composites based on their tensile response. Mater Struct. 2006;39:547-55.

[3] di Prisco M, Colombo M, Dozio D. Fibre-reinforced concrete in fib Model Code 2010: principles, models and test validation. Structural Concrete. 2013;14:342-61.

[4] Mazaheripour H, Barros JAO, Soltanzadeh F, Gonçalves DMF. Interfacial bond behaviour of GFRP bar in self-compacting fiber reinforced concrete. In: al Be, editor. 8th RILEM International Symposium on Fibre Reinforced Concrete: challenges and opportunities (BEFIB2012). Guimaraes2012. p. 135-6.

[5] Mazaheripour H, Barros JAO, Sena-Cruz JM, Pepe M, Martinelli E. Experimental study on bond performance of GFRP bars in self-compacting steel fiber reinforced concrete. Composite Structures. 2013;95:202-12.

[6] van Mier JGM. Fracture Processes of Concrete: CRC Press; 1997.

[7] Koshikawa T. Modelling the postpeak stress-displacement relationship of concrete uniaxial compression. In: al VMe, editor. Proc of VII International Conference on Fracture Mechanics of Concrete Structures (FraMCoS-8)2013.

[8] Haskett M, Oehlers DJ, Mohamed Ali MS, Sharma SK. Evaluating the shear-friction resistance across sliding planes in concrete. Engineering Structures. 2011;33:1357-64.

[9] Vandewalle L, et al. Test and design methods for steel fibre reinforced concrete - Final Recommendation. Mater Struct. 2002;35:579-82.

[10] fib Model Code 2010 - Final draft: CEB and FIP; 2011.

[11] Haskett M, Oehlers DJ, Mohamed Ali MS, Wu C. Rigid body moment–rotation mechanism for reinforced concrete beam hinges. Engineering Structures. 2009;31:1032-41.

[12] Haskett M, Oehlers D, Mohamed Ali M, Wu C. Yield Penetration Hinge Rotation in Reinforced Concrete Beams. Journal of Structural Engineering. 2009;135:130-8.

[13] Visintin P, Oehlers D, Haskett M, Wu C. Mechanics-Based Hinge Analysis for Reinforced Concrete Columns. Journal of Structural Engineering. 2013;139:1973-80.

[14] Visintin P, Oehlers DJ, Wu C, Haskett M. A mechanics solution for hinges in RC beams with multiple cracks. Engineering Structures. 2012;36:61-9.

[15] Visintin P, Oehlers DJ, Muhamad R, Wu C. Partial-interaction short term serviceability deflection of RC beams. Engineering Structures. 2013;56:993-1006.

[16] Esmaeeli E, Manning E, Barros JAO. Strain hardening fibre reinforced cement composites for the flexural strengthening of masonry elements of ancient structures. Construction and Building Materials. 2013;38:1010-21.

[17] Pereira EB, Fischer G, Barros JAO. Direct assessment of tensile stress-crack opening behavior of Strain Hardening Cementitious Composites (SHCC). Cement and Concrete Research. 2012;42:834-46.

[18] Barros JAO, Salehian H, Pires NMMA, Gonçalves DMF. Design and testing elevated steel fibre reinforced self-compacting concrete slabs. Eighth RILEM International Symposium on Fibre Reinforced Concrete (BEFIB2012): Challenges and opportunities. Guimaraes, Portugal2012.

[19] Shah SP, Swartz SE, Ouyang C. Fracture mechanics of concrete: applications of fracture mechanics to concrete, rock and other quasi-brittle materials: John Wiley & Sons, Inc; 1995.

[20] Cunha VMCF, Barros JAO, Sena-Cruz JM. Modelling the influence of age of steel fibre reinforced self-compacting concrete on its compressive behaviour. Mater Struct. 2008;41:465-78.

[21] Vipulanandan C, Paul E. Performance of epoxy and polyester polymer concrete. ACI Materials Journal. 1990;87:241-51.

[22] Barros J, Figueiras J. Flexural Behavior of SFRC: Testing and Modeling. Journal of Materials in Civil Engineering. 1999;11:331-9.

[23] Visintin P. A generic segmental analysis of all type of RC members. Adelaide, Australia: Adelaide; 2012.

[24] Divakar M, Fafitis A, Shah S. Constitutive Model for Shear Transfer in Cracked Concrete. Journal of Structural Engineering. 1987;113:1046-62.

[25] Fujita Y, Ishimaru R, Hanai S, Suenaga Y. Study on internal friction angle and tensile strength of plain concrete. Third International Conference on Fracture Mechanics of Concrete and Concrete Structures (FRAMCOS-3). Gifu, Japan: AEDIFICATIO Publishers; 1998. p. 325-34.

[26] Bianco V, Barros J, Monti G. Bond Model of NSM-FRP Strips in the Context of the Shear Strengthening of RC Beams. Journal of Structural Engineering. 2009;135:619-31.

[27] Qureshi J. Modelling of stress transfer across reinforced concrete interfaces: University of Tokyo; 1993.

[28] Taheri M, Barros JAO. An analytical model to simulate tension stiffening mechanism in moment-rotation response of FRC flexural members with tensile longitudinal reinforcement. Guimaraes, Portugal: University of Minho; 2012. p. 34.

[29] Barros JAO, Taheri M, Salehian H, Mendes PJD. A design model for fibre reinforced concrete beams pre-stressed with steel and FRP bars. Composite Structures. 2012;94:2494-512.

[30] Barros JAO, Santos SPF, Lourenço LAP, Gonçalves DMF. Flexural behaviour of steel fibre reinforced self-compacting concrete laminar structures. In: Barragán B, Pacios A, Serna P, editors. 1st Spanish Congress on Self-Compacting Concrete (HAC2008). Valencia2008. p. 567-78.

[31] Vandewalle L. Cracking behaviour of concrete beams reinforced with a combination of ordinary reinforcement and steel fibers. Mater Struct. 2000;33:164-70.

[32] Tan K-H, Paramasivam P, Tan K-C. Cracking characteristics of reinforced steel fiber concrete beams under short- and long-term loadings. Advanced Cement Based Materials. 1995;2:127-37.

[33] Moraes Neto BN, Barros JAO, Melo GSSA. A model for the prediction of the punching resistance of steel fibre reinforced concrete slabs centrically loaded. Construction and Building Materials. 2013;46:211-23.

[34] Harajli M, Hamad B, Karam K. Bond-slip Response of Reinforcing Bars Embedded in Plain and Fiber Concrete. Journal of Materials in Civil Engineering. 2002;14:503-11.

Notation

A	=	constant coefficient
$A_{c,eff}$	=	effective area in tension
A_s	=	cross sectional area of steel bar
$A_{s,c}$	=	area of reinforcement in compression zone
$A_{s,t}$	=	area of reinforcement in tension zone
a	=	distance between load point and support
B	=	constant coefficient
b	=	beam width
b_i	=	width of *ith* layer
b_s	=	width of reinforcement
b_c	=	width of surrounding concrete of reinforcement
C	=	cover of reinforcement
d_s	=	central distance of steel bars from top face of section
d_f	=	diameter of fibre
d_{cr}	=	distance of crack apex from top face of section
d_i	=	depth of *ith* layer
d_{NA}	=	depth of neutral axis
d_{wd}	=	Depth of wedge
D_i	=	horizontal deformation at *ith* layer
E_c	=	modulus of elasticity of FRC
$E_{c,\sec}$	=	secant modulus of elasticity of FRC
E_s	=	modulus of elasticity of steel bars
EI_k^i	=	flexural stiffness of the *ith* segment in the *kth* step of loading
F_j	=	force value corresponding to the $CMOD_j$
F_i^c	=	Force of FRC in layer *i*
F_{s1}	=	internal force of reinforcement at section1
F_i^s	=	internal force of reinforcement at layer *i*
f_{cc}	=	compressive strength of FRC
f_{ctm}	=	average value of the concrete axial tensile strength
f_{Ftsm}	=	average value of the residual flexural tensile strength parameter for serviceability limit state analysis of FRC
f_{ct}	=	tensile strength of concrete
f_{sy}	=	yielding stress of steel bar
f_{R1}	=	residual flexural tensile strength at a crack mouth opening displacement (CMOD) of 0.5 mm
f_{R3}	=	residual flexural tensile strength at a crack mouth opening displacement (CMOD) of 2.5 mm
h	=	beam depth
h_{sp}	=	distance between the tip of the notch and the top of the cross section
k	=	counter
k_i	=	non dimensional coefficients
k_{bs}	=	stiffness of linear bond-slip behaviour

L = beam total length
L_{cs} = crack spacing
L_{csm} = average crack spacing for members subjected to flexure or tension
$L_{cs,\max}$ = maximum crack spacing in R/FRC elements
L_{ps} = circumference of the reinforcement
l_f = length of fibre
M = bending moment
M_{cr} = cracking moment of the section
M_i = bending moment in stage *i*
M_k = moment of the prism section, corresponds to the imposed θ_k
n = number of layers
P = total applied load on beam
p = constant parameter
P_k = total applied load on beam in *kth* step of loading
q = constant parameter
S = relative displacement along the wedge plane
S_i = relative displacement along the wedge plane in layer *i*
s = sliding displacement
s_1 = sliding at section1
t_i = thickness of *ith* layer
t_s = thickness of reinforcement
u = axial component of the sliding
u_i = axial component of the sliding of layer*i*
V_f = volume fraction of fibres
w = crack width
w_d = design value of crack width
w_i = crack width of layer *i*
w_u = ultimate crack width
w_s = crack width at the level of reinforcement bar
W_f = fibre weight percentage in the mixture
α_i = normalized post cracking stress
β_s = constant coefficient
γ = angle of the wedge plane
γ_s = normalized modulus of elasticity of steel bars
δ = deflection
δ_k = mid-span deflection of the beam for the *kth* loading step
ε_{cc} = compressive strain of FRC
$\varepsilon_{cc,p}$ = strain corresponding to compressive strength
$\varepsilon_{cc,p}^{PC}$ = strain at compressive strength of the plain concrete
$\varepsilon_{cc,p}^{SFRC}$ = strain at compressive strength of the steel fiber reinforced concrete
$\varepsilon'_{cc,i}$ = compressive strain of layer when subjected to sliding of S_i.
$\varepsilon_{cc,1}$ = compressive strain at upper face of the prism section
ε_{cu} = ultimate compressive strain of FRC

ε_{cr}	=	tensile strain at crack initiation of FRC
ε_{ct}	=	tensile strain of FRC
ε_i^{ef}	=	effective strain of layer i
ε_s	=	strain of rebar at the onset of cracking
ε_{st}	=	tensile strain of steel bar
ε_{sy}	=	yielding strain of steel bar
ε_{su}	=	ultimate tensile strain of steel bar
ε_{sm}	=	mean strain in the reinforcement between the cracks
$\rho_{s,ef}$	=	effective reinforcement ratio
ρ	=	reinforcement ratio of longitudinal steel bars
σ	=	stress
σ_{cc}	=	compressive stress of FRC
σ_{ct}	=	tensile stress of FRC
$\sigma_{ct}(w_s)$	=	tensile stress-crack width response of FRC
σ_{st}	=	tensile stress of the steel bars
σ_{sr}	=	the maximum steel stress in a crack in the crack formation stage
σ_1	=	normal stress at wedge plane
τ	=	bond stress
τ_{bm}	=	average bond strength between reinforcing bars and concrete
τ_1	=	shear stress at wedge plane
χ	=	curvature
χ_k^i	=	curvature of the *ith* segment in the *kth* step of loading
χ_k	=	Curvature of beam corresponding to the imposed θ_k
θ	=	rotation of section
θ_k	=	imposed rotation at *kth* step
ϕ	=	bar diameter
$\Delta\theta$	=	increment of rotation

List of tables:

List of Figures:

Fig. 19 - Effect of the k_{bs} bond stiffness on the: (a) load-deflection, and (b) load-crack width responses of R/FRC beams.